

# Complete coherent control of silicon vacancies in diamond nanopillars containing single defect centers: supplementary material

JINGYUAN LINDA ZHANG,<sup>1,7,‡</sup> KONSTANTINOS G. LAGOUDAKIS,<sup>1,6,‡</sup> YAN-KAI TZENG,<sup>4</sup> CONSTANTIN DORY,<sup>1</sup> MARINA RADULASKI,<sup>1</sup> YOUSIF KELAITA,<sup>1</sup> KEVIN A. FISCHER,<sup>1</sup> SHUO SUN,<sup>1</sup> ZHI-XUN SHEN,<sup>2,3,4</sup> NICHOLAS A. MELOSH,<sup>2,3</sup> STEVEN CHU,<sup>4,5</sup> JELENA VUČKOVIĆ<sup>1</sup>

<sup>1</sup>E. L. Ginzton Laboratory, Stanford University, Stanford, California 94305, USA

<sup>2</sup>Geballe Laboratory for Advanced Materials, Stanford University, Stanford, California 94305, USA

<sup>3</sup>Stanford Institute for Materials and Energy Sciences, SLAC National Accelerator Laboratory, Menlo Park, California 94025, USA

<sup>4</sup>Department of Physics, Stanford University, Stanford, California 94305, USA

<sup>5</sup>Department of Molecular and Cellular Physiology, Stanford University, Stanford, California 94305, USA

<sup>6</sup>e-mail: [lagous@stanford.edu](mailto:lagous@stanford.edu)

<sup>7</sup>e-mail: [ljzhang@stanford.edu](mailto:ljzhang@stanford.edu)

<sup>‡</sup>These authors contributed equally.

Published 23 October 2017

This document provides supplementary information to “Complete coherent control of silicon vacancies in diamond nanopillars containing single defect centers,” <https://doi.org/10.1364/optica.4.001317>.

<https://doi.org/10.6084/m9.figshare.5439571>

## Density, Yield, and Conversion Efficiency of SiV Centers in Nanopillar Arrays

We conduct a statistical study of SiV<sup>-</sup> center spectra in the nanopillars to characterize the density of SiV<sup>-</sup> centers and the yield of single SiV<sup>-</sup> centers in nanopillar devices (Figure S1). The number of SiV<sup>-</sup> centers in each nanopillar can be identified by the number of radiative transitions in the PL spectra. The inhomogeneous distribution and the possible presence of strain-induced spectral shifting of some of the SiV<sup>-</sup> centers helps identify different SiV<sup>-</sup> centers in individual nanopillars. Out of the 64 nanopillars investigated within the entire array, 31.3% contain a single SiV<sup>-</sup> while 6.3% contain two SiV<sup>-</sup> centers. Based on the measured dimensions and the average number of SiV<sup>-</sup> centers per nanopillar, we estimate the density of SiV<sup>-</sup> centers in the epilayer to be  $3 \times 10^{14} \text{ cm}^{-3}$ .

In principle, the conversion efficiency of silicon to SiV can be obtained by measuring the density of the incorporated silicon atoms through Secondary Ion Mass Spectroscopy (SIMS). However, the SIMS technique is a “destructive” measurement and results in the sputtering of material. In addition, the low density of the silicon atoms makes it difficult to achieve good signal to noise ratio for the

SIMS measurement. For these reasons, we have not experimentally obtained the conversion efficiency using this MPCVD growth method. However, a high Si concentration may lower the spin coherence due to the nuclear spin-bath of the <sup>29</sup>Si (4.7% natural abundance).

## Second-Order Autocorrelation

Measuring the second-order autocorrelation function  $g^{(2)}(\tau)$  confirms the quantum nature of light emitted by the individual SiV<sup>-</sup> centers in nanopillars (Figure S2). In the representative  $g^{(2)}(\tau)$ , the SiV<sup>-</sup> center is excited above saturation, and the signal is fitted with  $g^{(2)}(\tau) = 1 - (1 + a)e^{-|\tau|/\tau_1} + ae^{-|\tau|/\tau_2}$  convolved with the measured instrument response function (IRF), yielding  $g^{(2)}(0) = 0.29$ . Deconvolution of the instrument response function from the  $g^{(2)}(\tau)$ , as shown by the green curve in Fig. S2, yields  $g^{(2)}(0) = 0.04$  for an ideal instrument response, which indicates that the timing jitter of the detector largely accounts for the non-ideality of the second order correlation measurement.

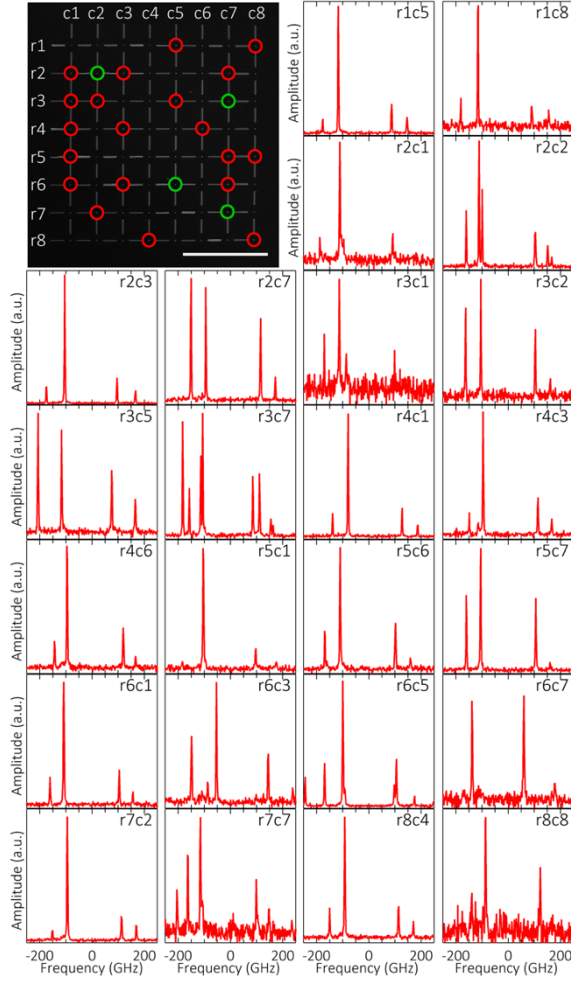


Figure S1. Statistical study of the SiV- center distribution in the nanopillars by PL spectroscopy. The red (green) circles indicate the nanopillars containing single (double) SiV- centers, while the PL spectra of SiV- centers in the nanopillars are shown in the insets.

The measured  $g^{(2)}(0) < 0.5$  supports the conclusions from the spectroscopic study that the SiV- center under coherent control by the ultrafast optical pulses was indeed a single color center.

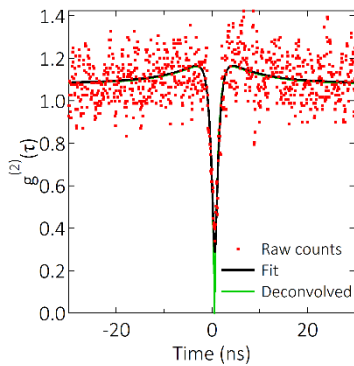


Figure S2. Second-order autocorrelation function  $g^{(2)}(\tau)$  of the coherently controlled SiV- center, yielding  $g^{(2)}(0) = 0.29$  after convolving the fitted function with the instrument response function (black), and  $g^{(2)}(0) = 0.04$  with the instrument response function deconvolved from the fit (green).

### Spectral Overlap of Single SiV Centers in Nanopillars

Within the 8 by 8 array reported in Figure S1, several of the nanopillars with individual SiV centers contain minimally stressed emitters that show strong spectral overlap, as shown in Figure S3. These spectra demonstrate the potential for indistinguishability experiments of the developed platform.

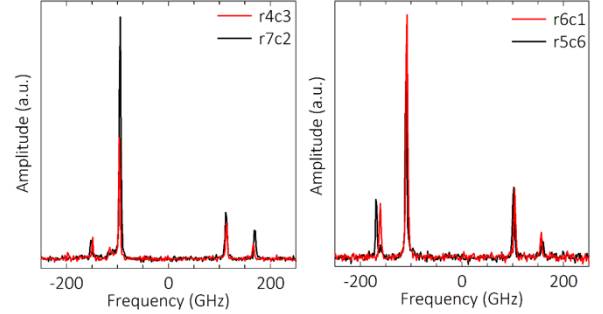


Figure S3: Photoluminescence spectra of SiV centers from two pairs of nanopillars show significant spectral overlap in the strongest emission transition, showing promise for indistinguishable photons from different nanopillars. These nanopillars are from the same 8 by 8 array shown in Figure S1.

### Inhomogeneous Distribution, Linewidth and Orbital-State Splitting of Single SiV Centers in Nanopillars

To quantify the transition energy inhomogeneity in the nanopillars, we find the average photoluminescence spectrum of individual single SiV centers in 300 nanopillars, contrasting that with the PL spectrum from SiV ensemble in bulk diamond, as shown by the red and blue curves respectively in Figure S4. The inhomogeneous distribution of transition C in the nanopillars containing single SiV (red curve) is  $\sim 38$  GHz, whereas that in the bulk area (blue curve) on the same sample is  $\sim 15$  GHz. The spectrometer resolution limited linewidth of the single SiV center studied in this work is 2.4GHz.

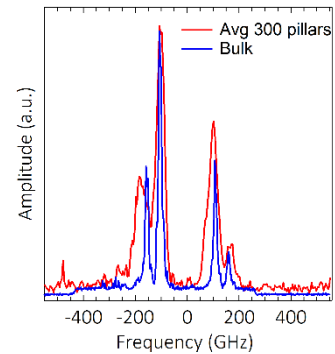


Figure S4: Averaged PL spectrum from 300 nanopillars containing single SiV center (red), compared with the PL spectrum from ensemble in bulk diamond (blue).

The ground/excited orbital-state splittings for (i) “bulk” ensemble, (ii) the single SiV center studied here, and (iii) the summation of many single SiV spectra are (i) 49.2/265 GHz, (ii) 79.6/276GHz, and (iii) 77.3/280 GHz, respectively. The energy splittings for the “bulk” ensemble are similar to those previously reported for zero-strain

SiVs, while those in nanopillars are greater than the zero-strain SiVs, indicating the presence of some level of strain.

### Brightness of Single SiV Centers

We have not been able to saturate the emitters in nanopillars with our available excitation laser power under 532 nm excitation. However, we can extract the count rate under  $\pi$  pulse excitation by characterizing the collection efficiency through our set-up and the simulated collection efficiency of the emission from an emitter located inside a nanopillar into the light cone of the objective. The photon detection efficiency of the SPCM at 740 nm is  $\sim 60\%$ . The transmission through the first and second monochromators are  $\sim 45\%$  and  $40\%$  respectively. The transmission through the optics of the set-up is  $\sim 52\%$ . The simulated collection efficiency of emission into an NA=0.7 light cone is  $\sim 7\%$  (Figure S5). From these parameters, we extract the emission rate into zero phonon line C to be  $29 \text{ kcs}^{-1}$ . Contrasting that with the count rates of  $56 \text{ kcs}^{-1}$  for SiV centers in bulk and  $730 \text{ kcs}^{-1}$  collected through an NA=0.95 objective.<sup>1</sup> The deviation may come from the different NA objectives used, and the effect of possible static strain on the fraction of light emission into the zero-phonon line.

We have performed the electromagnetic simulation of radiation pattern using the finite-difference-time-domain (FDTD) method. The collection efficiency of emission into an NA=0.7 light cone as a function of the emitter depth within the doped layer is shown by the red curve in Figure S5. The collection efficiency of the photoluminescence from an emitter located at the center of the doped region (depth=50 nm) into a microscope objective with NA=0.7 is 7.6%. Contrasting that with  $\sim 3\%$  collection efficiency for bulk and  $\sim 20\%$  for SIL into an objective with similar NA.<sup>2</sup> We have simulated the collection efficiency for several common color centers (NV<sup>-</sup>, SiV<sup>-</sup>, Cr, SiV<sup>0</sup>), and the collection efficiency dependence on the wavelength is shown by the different colored curves in the same figure.

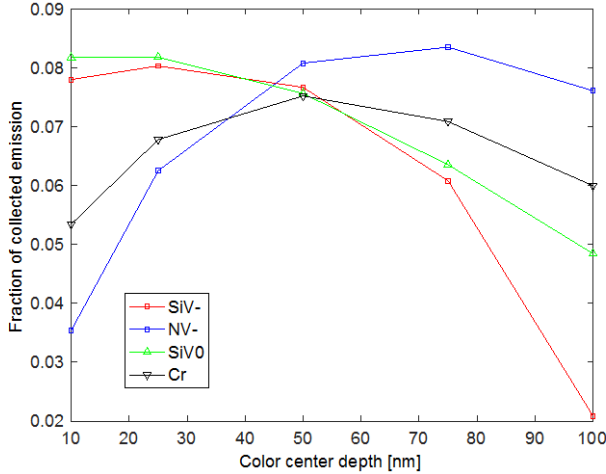


Figure S5: Fraction of photons collected into a microscope objective with NA=0.7 for various emitter depths.

### Quantum Optics Simulation

We perform the modeling using the Quantum Toolbox in Python (QuTiP). We model the system with a simplified model of a two-level system consisting of the upper excited state and upper ground state with energy splitting  $\omega_0$ . The driving laser field is resonant with the two level system,  $\omega_l = \omega_0$ . The system is described by the Hamiltonian

$$\mathcal{H} = \omega_{gs}|0\rangle\langle 0| + (\omega_0 - \omega_l)|1\rangle\langle 1| + \Omega(|0\rangle\langle 1| + |1\rangle\langle 0|)(1 + e^{i\omega_l \Delta t}),$$

where  $\omega_{gs} = 0$  is the ground state energy,  $\Omega$  is the excitation laser field, and  $\Delta t$  is the interpulse delay. The last term of the Hamiltonian corresponds to the interaction between the field and the emitter.

The dynamics of the SiV is solved by solving the master equation in Lindblad form:  $\frac{d\rho}{dt} = \frac{i}{\hbar}[\rho, \mathcal{H}] + \mathcal{L}(\rho)$ , where  $\rho$  is the density matrix of the SiV, and  $\mathcal{L}(\rho)$  is the Lindblad superoperator capturing the system relaxation due to coupling to the environment. The relaxation mechanisms include the radiative decay from the excited state to the ground state with independently measured  $\gamma_1 = \frac{1}{T_1} = 0.58 \text{ GHz}$ , a fitted excited state dephasing rate  $\gamma_{ph} = 5 \text{ GHz}$ , and a fitted power dependent excited state dephasing rate  $\gamma_p = 5 \text{ GHz}$ .

### REFERENCES

1. L. J. Rogers, K. D. Jahnke, T. Teraji, L. Marseglia, C. Muller, B. Naydenov, H. Schauffert, C. Kranz, J. Isoya, L. P. McGuinness, F. Jelezko, "Multiple intrinsically identical single-photon emitters in the solid state," *Nat Commun* **5**, 4739 (2014).
2. C. J. Hepp, *Electronic Structure of the Silicon Vacancy Color Center in Diamond* (Universität des Saarlandes, 2014).